Society of Medical Education & Research

2024, Volume 4, Issue 2, Page No: 141-158
ISSN: 3108-4834

Archive of International Journal of Cancer and Allied Science

Differential Presentation and Immunogenicity of Phosphopeptides by Common HLA Alleles in Leukemia and Lymphoma

Thabo Sipho Dlamini[1]*, Nomvula Grace Moyo[1]

[1]Division of Medical Oncology, University of Cape Town, Cape Town, South Africa.

***E-mail** ✉ t.dlamini.uct@gmail.com

Abstract

Aberrant phosphorylation in cancer cells results in the selective presentation of phosphorylated peptides by MHC molecules. Peptides bound to HLA-A*02:01 demonstrate greater stability compared to their nonphosphorylated forms, which may enhance immune recognition. However, it remains uncertain if phosphopeptides displayed by other common alleles share similar structural or immunogenic traits. To investigate this, we analyzed the identity, structure, and immunogenic potential of phosphopeptides presented by HLA-A*03:01, -A*11:01, -C*07:01, and -C*07:02. We performed immunoprecipitation to isolate peptide-MHC complexes from 10 healthy and tumor tissue samples and analyzed them via mass spectrometry. The resulting dataset was merged with publicly available immunopeptidomics data to form a curated set of phosphopeptides from 20 different healthy and cancerous tissue types. Selected phosphopeptides were assessed for biochemical characteristics using in vitro binding assays and computational docking, and their ability to elicit T cell responses was tested through multimer binding and cytokine analysis in T cells from healthy donors. We found phosphopeptides presented by HLA-A*03:01, -A*11:01, -C*07:01, and -C*07:02 across multiple tumor types, especially leukemias and lymphomas, but not in normal tissues. These peptides originated from genes critical for tumor cell survival. Phosphopeptides generally bound HLA-A*03:01 as well as or worse than their unmodified counterparts, while HLA-C*07:01 selectively presented phosphorylated peptides but rarely their unmodified forms. Binding to HLA-C*07:01 relied on interactions in the B-pocket, which were missing in HLA-C*07:02. T cells recognizing HLA-A*02:01 and -A*11:01 phosphopeptides were detectable in autologous settings even in the presence of the nonphosphorylated peptide, whereas HLA-A*03:01 and -C*07:01 phosphopeptides required allogeneic T cells for T cell activation. Phosphopeptides presented on multiple alleles that are tumor-specific could serve as immunotherapy targets, but not all are inherently immunogenic. Peptides presented by HLA-A*02:01 and -A*11:01 consistently triggered T cell responses, whereas those associated with HLA-A*03:01 and -C*07:01, though presented, did not. Therefore, allele-specific differences should be considered when designing phosphopeptide-targeted therapies for broader patient coverage.

Keywords: Phosphopeptides, Tumor antigens, Immunotherapy, Immunogenicity, Leukemia, Lymphoma

Introduction

T cells targeting tumor-specific antigens in the context of MHC can produce durable tumor regression, even in treatment-resistant cancers, through adoptive transfer. Proper antigen selection is crucial for achieving remission and preventing relapse. Neoantigens arising from nonsynonymous somatic mutations are tumor-specific but typically patient-specific and more abundant in tumors with higher mutational burdens. Differentially expressed tumor-associated antigens, such as WT1, Survivin, PRAME, and NYESO1, have been safely exploited to treat various pediatric and hematologic malignancies [1–3], which often lack sufficient neoantigens due to low mutation rates. A critical

Access this article online https://smerpub.com/

Received: 29 May 2024; **Accepted:** 29 October 2024

How to cite this article: Dlamini TS, Moyo NG. Differential Presentation and Immunogenicity of Phosphopeptides by Common HLA Alleles in Leukemia and Lymphoma. Arch Int J Cancer Allied Sci. 2024;4(2):141-58. https://doi.org/10.51847/RY5g9bhr57

limitation is that not all immunogenic peptides are naturally presented by tumor cells. Mass spectrometry now allows direct identification of peptides eluted from HLA immunoprecipitates (HLA-IP) [4]. Using HLA-IP and MS, researchers have identified post-translationally modified peptides, including phosphopeptides [5] and glycopeptides [6], as promising tumor antigens.

Certain phosphopeptides presented by specific HLA class I and II alleles show elevated immunogenicity, likely due to distinctive structural properties [7–9]. Cobbold *et al*. reported that healthy donors possess T cell responses against these phosphopeptides, while leukemic patients do not [10], a deficiency that is restored following allogeneic stem cell transplantation. Colorectal cancer patients also exhibit TILs and peripheral T cells with elevated recognition of phosphopeptides compared to healthy individuals [11], resembling patterns observed with somatic mutation-derived neoantigens [12, 13].

To broaden the repertoire of phosphopeptides suitable for immunotherapy, we applied HLA-IP to 10 hematologic cell line samples and integrated the data with public immunopeptidomics datasets. This yielded a set of phosphopeptides not present in normal tissues. From this set, we selected peptides presented by HLA-A*03:01, -A*11:01, and -C*07:01 and evaluated their binding stability, structural characteristics, and T cell activation potential, identifying promising candidates for future therapeutic development.

Materials and Methods

Cells

T2 cells, EBV-transformed B lymphoblastoid lines (EBV-BLCL), and monoclonal EBV-associated lymphoma cells (EBV-LPD) emerging after marrow transplantation were propagated in RPMI medium with 10% fetal bovine serum, 2 mM L-Glutamine, and penicillin-streptomycin. To generate T2 lines expressing specific HLA alleles, HLA-A*03:01, HLA-C*07:01, and HLA-C*07:02 cDNAs (IDT) were cloned into the pSBbi-GP plasmid [14] (Addgene #60511) using NEBbuilder HiFi Assembly. Correct ligation was verified by Sanger sequencing of DH5α (NEB) colonies carrying the ligation product. Stable transfection of T2 cells was achieved by co-delivering 4.5 µg of HLA-pSBbi-GP and 0.5 µg of pCMV(CAT)T7-SB100 [15] (Addgene #34879), followed by puromycin selection.

HLA ligand isolation and identification

Peptides bound to HLA molecules were captured and sequenced via immunoprecipitation followed by LC-MS/MS according to established methods [16]. Around 1–2×10^8 cells were washed in PBS, snap-frozen, and stored at −80°C. Pellets were thawed on ice and lysed for 1 hour at 4°C in 1% CHAPS in PBS with cOmplete protease inhibitors and PhosSTOP. Lysates were clarified by centrifugation, and supernatants were circulated overnight at 4°C through W6/32-conjugated sepharose for MHC class I, or L243-/IVA12-conjugated sepharose for class II, using a peristaltic pump. Peptide-HLA complexes were eluted in 1% trifluoroacetic acid, applied to pre-equilibrated Sep-Pak tC18 columns (80% ACN), and eluted with either 40% ACN/0.1% TFA or 30% ACN/0.1% TFA. Solid-phase extraction was performed using in-house C18 minicolumns (Empore), washed, equilibrated, loaded with eluates, and desalted with 80% ACN/0.1% TFA. Peptides were analyzed on a Lumos Fusion mass spectrometer in data-dependent acquisition mode. Separation was done on a 12-cm emitter column with a 70-minute gradient (2–30% B; B = 80% ACN/0.1% formic acid). The injection volume was 3 µL of 8 µL. Peptide charge states 3+ and 4+ (and undetermined) were scanned in m/z 250–700, 2+ peptides in m/z 350–1000, and 1+ peptides in m/z 750–1800.

T2 stabilization assay

T2 cells expressing the relevant HLA allele were harvested and incubated at room temperature for 18 hours. Cells were washed with PBS and resuspended in serum-free RPMI with 3 µg/mL β2-microglobulin (MP Biomedicals) and the designated peptide concentration. The incubation continued for 3 hours at room temperature and 3 hours at 37°C in 5% CO2. After washing, cells were stained for 30 minutes at 4°C using FVD Violet (1:1000), HLA-A2 PE (BD, 1:100), HLA-A3 PE-Vio770 (Miltenyi, 1:100), or HLA-C AF647 (BioLegend, 1:100). Cells were washed twice and analyzed on a BD LSRII.

Molecular docking

Peptide-HLA docking followed previously described procedures [17]. Crystal structures from the PDB were used as templates. PDB 5VGE was employed for docking 9-mers to HLA-C*07:02, and 3RL1 and 3RL2 were templates for 9- and 10-mers with HLA-A*03:01. To model HLA-C*07:01, K66N and S99Y mutations were introduced using UCSF Chimera [18]. Peptides were

threaded using Dunbrack and SwissSideChain rotamer libraries [19, 20]. Prepacking and docking used FlexPepDock in Rosetta3 [21, 22] in refinement mode. For each peptide-HLA pair, 200 high-resolution models were generated, scored using the ref2015 full-atom function in Rosetta energy units (REU), and the 10 lowest-scoring models were selected. Chimera was used to visualize structures and examine hydrogen bonding.

Immunogenicity assessment

The ability of phosphopeptides to trigger immune responses was tested using either ELISpot assays or multimer staining on HLA-typed donor PBMC. Each donor's PBMC was exposed to peptides selected according to their HLA profile, following the procedure described previously [4]. For dendritic cell-mediated priming, the method of Wölfl & Greenberg [23] was applied. In some experiments, autologous peptide-loaded CD14+ cells or T2 cells expressing the corresponding HLA allele were used instead of dendritic cells. Between 10 and 13 days after initial stimulation, cells were re-exposed to peptide-pulsed, lethally irradiated autologous PBMC, dendritic cells, or T2 cells, and maintained in medium supplemented with IL7 and IL15 at 5 ng/mL, along with IL2 (Miltenyi) at 50 IU/mL. Cultures were maintained in Xvivo-15 medium (Lonza) containing 5% human AB serum (Gemini). Analysis was generally performed on days 10–13 of each stimulation cycle using multimer staining or ELISpot against autologous peptide-pulsed targets, as previously reported [24–26].

Dextramer reagents were assembled according to our in-house protocol [27], adapted from earlier work [28]. For enrichment, 1–3×10^8 PBMC were pretreated with 50 nM dasatinib and Fc receptor blocking reagent for 30 minutes at 37°C, followed by incubation with 10 µg/mL of the designated dextramer pool for 1 hour at 4°C. Cells were sequentially captured using anti-Cy5, -PE, or -Cy7 magnetic beads (Miltenyi) over two LS columns. Following enrichment, cells were either stained for surface markers and immediately analyzed by flow cytometry, or expanded in 96-well plates with irradiated allogeneic feeder cells and anti-CD3/CD28 stimulation (STEMCELL) in the presence of IL2 (300 IU/mL), IL7 (5 ng/mL), and IL15 (5 ng/mL) for 10–14 days before subsequent analysis or further enrichment and expansion. For flow cytometric acquisition, the full volume of dextramer-enriched samples was collected.

Data analysis and statistics

Flow cytometry datasets were processed using FCS Express (De Novo Software), while all other analyses were performed using custom Python and R scripts. Paired t-tests were applied for statistical evaluation. Genetic dependency information was retrieved from the DepMap portal [29] (www.depmap.org/), and DEMETER2 scores were averaged per gene across groups of cell lines using custom Python scripts. Gene ontology (GO) enrichment analysis was conducted using STRING (www.string-db.org). Peptide-HLA binding predictions were generated with NetMHCpan4.0, and peptide motif clustering was performed with GibbsCluster-2.0. Mass spectrometry data from prior studies [4, 30–32] were obtained through ProteomeXchange (accession numbers: PXD004746, PXD005704, PXD012083, PXD013831).

Results and Discussion

Characterization of tumor-specific immunogenic phosphopeptides. We aimed to map the phosphopeptidome associated with prevalent HLA alleles beyond A*02:01 to identify cancer antigens displayed exclusively on malignant cells and absent from normal tissues. Given prior evidence of phosphopeptide presentation on EBV-transformed B-lymphoblastoid cell lines, we performed HLA class I and class II immunoprecipitation followed by LC-MS/MS to recover HLA-bound ligands from 6 EBV-BLCL lines, 2 AML lines (treated with either decitabine for enhanced antigen processing or DMSO), 1 EBV-LPD line, and 1 normal B cell sample. Limiting identifications to peptides ≥8 mers with a strict 1% FDR and DeltaMod ≥20 in Byonic [33], we obtained 40,557 unique non-phosphorylated peptides and 255 unique phosphopeptides across the dataset. Class I complexes yielded 214 unique phosphopeptides from 194 source proteins, while class II yielded 53 unique phosphopeptides from 37 proteins. EBV-transformed lines (EBV-BLCL and EBV-LPD) ranked highest in unique unmodified and phosphorylated peptide recovery **(Figure 1a)**. Class I phosphopeptides were predominantly 9-mers, and class II were mostly 16-mers **(Figure 1b)**, aligning with earlier reports [8, 32]. To compare phosphopeptidomes between malignant and healthy B cells in an autologous context, we analyzed class I ligands eluted from matched EBV-BLCL and healthy B cells from donor AP. Restricting to NetMHCpan4-predicted percentile rank ≤2% per expressed allele, HLA-A*11:01 emerged as the dominant

presenter of high-affinity binders in this donor, with most falling below the standard 500 nM threshold (dashed lines), **(Figure 1c)**. EBV-BLCL from donor AP presented over twice as many predicted high-affinity peptides as autologous healthy B cells (5,789 vs. 2,142); **(Figure 1c)**. Phosphopeptides (grey circles), **(Figure 1c)** were consistently more abundant across alleles in EBV-BLCL than in matched healthy B cells **(Figure 1d)**. Sequence-based assignment via NetMHCpan4.0 attributed the majority of these phosphopeptides to HLA-A*11:01. Overlap analysis across all 6 HLA-A*11:01-positive samples **(Figure 1e)** revealed novel phosphopeptides pGTF3C2, pPPP1R12A, pPIM1, pMYBBP1A, and pSRRM1 presented by multiple EBV-BLCL and EBV-LPD samples but absent from healthy B cells. Drawing from evidence of phosphopeptide immunogenicity in A*02:01-positive individuals [10, 17, 34], we investigated whether HLA-A*11:01 donors possess cognate T cells. From donor AP's EBV-BLCL eluates, only pGTF3C2 triggered specific IFNγ secretion from in vitro-sensitized T cells **(Figure 1f)**, whereas the unmodified GTF3C2wt failed to do so. Tetramer staining of donor AP PBMCs after one pGTF3C2 stimulation confirmed expansion of phosphopeptide-specific T cells **(Figure 1g).** To account for this selectivity, we applied FlexPepDock [21] molecular docking, as previously used for an A2-restricted pIRS2-specific TCR-mimic antibody [17], evaluating the 10 lowest-energy models for pGTF3C2 and GTF3C2wt bound to HLA-A*11:01 **(Figure 1h)**. Both complexes showed comparable energy scores and backbone conformations, consistent with GTF3C2wt's strong predicted binding (0.19% rank) and its co-detection by MS. However, the phosphorylated Ser at position 4 in pGTF3C2 conferred greater solvent exposure **(Figure 1h),** (left), likely enhancing TCR contact in the P4–P6 region and explaining its superior immunogenicity. Thus, select phosphopeptides are selectively displayed by HLA-A*11:01 on malignant cells and can elicit specific T cell responses in healthy donors despite co-presentation of the non-phosphorylated counterpart.

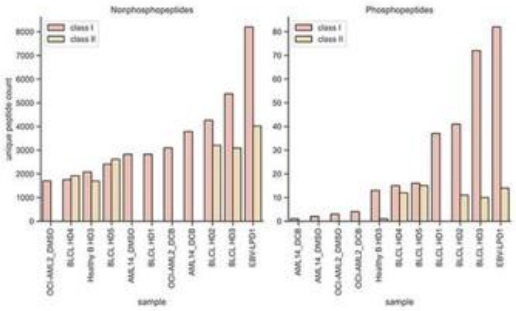

a)

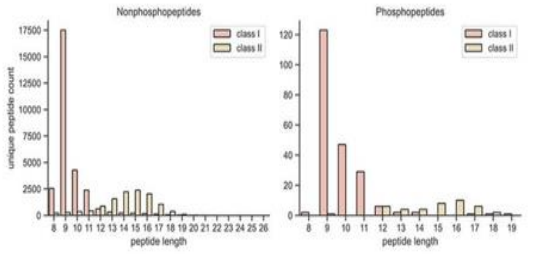

b)

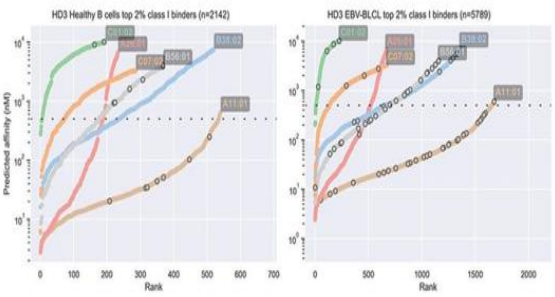

c)

HLA allele	Healthy B cell	EBV B Cell
A1101 unique binders	7	31
A2601 unique binders	0	1
B5601 unique binders	6	23
B3802 unique binders	0	7
C0702 unique binders	0	4
C0102 unique binders	2	4
Total unique phosphopeptides	13	73

d)

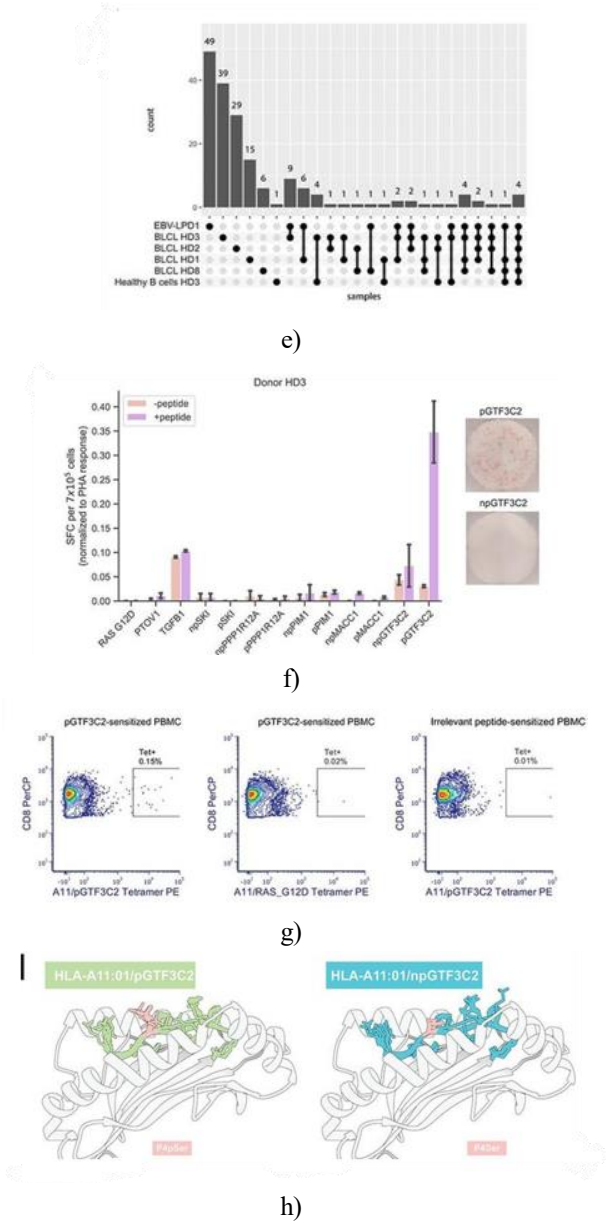

Figure 1. Recurrent, immunogenic phosphopeptides in the HLA-A11:01 immunopeptidome.

(a) Counts of unique peptides detected for class I and II non-phosphorylated peptides (left) and phosphopeptides (right) across all samples subjected to HLA-IP.

(b) Distribution of peptide lengths for class I and II non-phosphorylated peptides (left) and phosphopeptides (right).

(c) Predicted binding affinity (NetMHCpan4.0) versus rank for each HLA allele in healthy B cells (left) and EBV-BLCL (right) from donor AP. Grey circles denote phosphopeptides; the dashed line indicates a 500 nM binding threshold.

(d) Comparison of the total unique phosphopeptides between donor AP's healthy B cells and EBV-BLCL, shown in panel C.

(e) UpSet plot representing overlaps of phosphopeptides across all HLA-A11:01+ samples analyzed by HLA-IP.

(f) ELISpot assay of donor AP PBMC after sensitization with indicated peptides, reported as percent of PHA-stimulated control. Cultures were restimulated with either peptide-pulsed (+peptide) or unpulsed (−peptide) autologous PBMC. Representative images for pGTF3C2 and GTF3C2wt are shown.

(g) Tetramer staining of donor AP PBMC demonstrates an increased frequency of pGTF3C2-specific CD8 T cells after sensitization, compared with irrelevant tetramer (A11/RAS_G12D) or unrelated peptide-sensitized PBMC.

(h) Docking models of the 10 lowest-energy conformations of pGTF3C2 (left) and GTF3C2wt (right) bound to HLA-A*11:01, highlighting P4 Ser to illustrate the impact of phosphorylation on solvent exposure.

Expansion of phosphopeptide dataset reveals shared a3 supertype tumor antigens

We extended the phosphopeptide dataset using previous studies [4, 30–32], resulting in 2,466 unique phosphopeptides across 20 tissue types, including AML (n=19), mantle cell lymphoma (n=19), meningioma (n=18), and EBV-BLCL (n=13) **(Figure 2a)**. To further explore A*11:01, we analyzed phosphopeptides presented by HLA-A3 supertype alleles such as A*03:01 and A*11:77. We identified 772 phosphopeptides present in A3+ or A11+ samples but absent in other allele backgrounds, then assessed recurrence across all samples **(Figure 2b)**. Hierarchical clustering did not strictly group samples by tissue type or cancer origin, likely influenced by unequal tissue and allele representation.

Unsupervised clustering of 719 phosphopeptides ≥9 amino acids revealed two main sequence motifs: 68% featured P4 Ser and P5 Pro, consistent with known phosphopeptide preferences [4, 10, 32], while 32% contained repeated leucines, reflecting A*03:01 submotifs [35] **(Figure 2c).** Recurringly presented phosphopeptides for A3/A11 alleles are summarized in **Table 1**, most of which were detected in both A3+ and A11+ samples.

Kinase enrichment analysis [36] of parental genes for phosphopeptides found in at least two malignant A3/A11 samples—but absent from healthy tissue—highlighted

ATR, CDK2, and PRKDC as top upstream kinases, all associated with cell cycle control and DNA repair **(Figure 2d)**. Gene ontology analysis showed that these phosphopeptides are enriched for nucleic-acid binding proteins **(Figure 2e)**. Furthermore, recurrently presented phosphopeptides originated from genes critical for leukemia and lymphoma proliferation, including SRRM1, SRRM2, GTF3C2, and MYBBP1A **(Figure 2f).** These observations support the designation of selected phosphopeptides as shared tumor antigens derived from proteins essential for malignant cell survival.

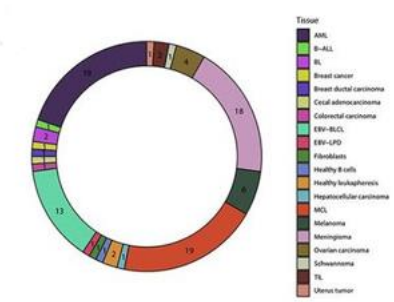

a)

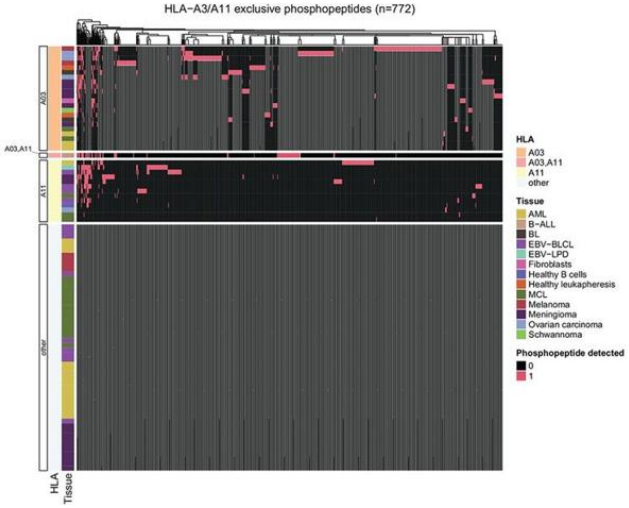

b)

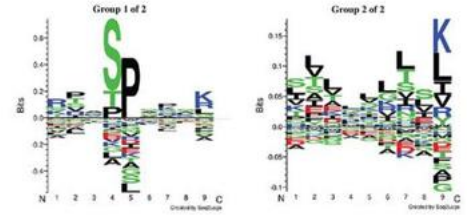

c)

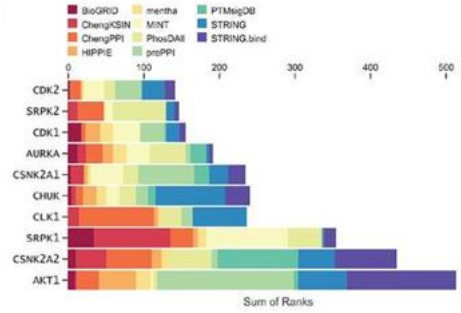

d)

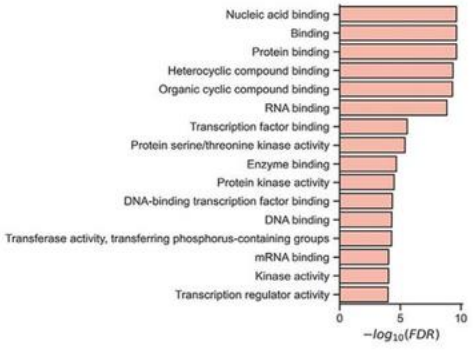

e)

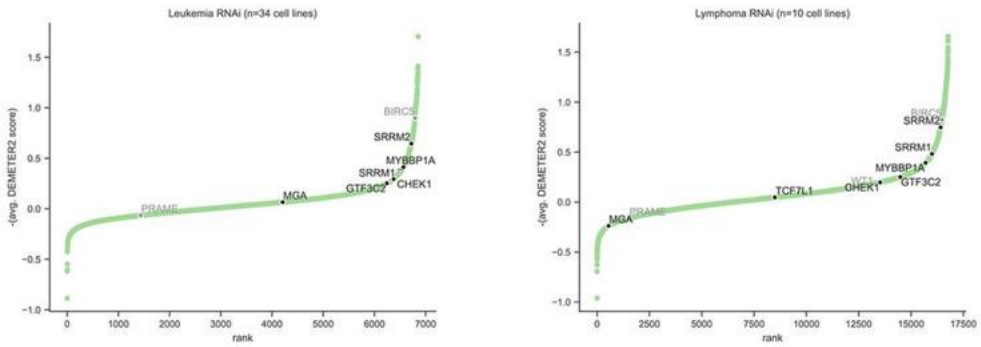

f)

Figure 2. Comprehensive analysis of the expanded phosphopeptide collection.
(a) Circular diagram depicting the distribution of tissue types included in the expanded dataset, with numbers indicating the count of unique samples per tissue category.
(b) Heatmap representing the presentation of phosphopeptides by HLA-A3 and HLA-A11 alleles. Rows correspond to individual tissue samples, and columns represent distinct phosphopeptides. HLA allele and tissue type for each sample are annotated on the left.
(c) Motif characterization of the phosphopeptides displayed in panel B, highlighting prevalent sequence patterns.
(d) Predicted upstream kinases associated with the parental genes of the phosphopeptides in panel B. Kinases are ordered by MeanRank, which decreases from bottom to top, and plotted against the total sum of ranks across kinase libraries, with library identity indicated by color.
(e) Gene ontology (GO) enrichment analysis of the parental genes corresponding to the phosphopeptides in panel b.
(f) Genetic dependency rank plots (−1 × average DEMETER2 score) for lymphoma and leukemia cell lines, derived from pooled RNAi screens [29]. Parental genes for the phosphopeptides are indicated, and known tumor-associated antigens Survivin (BIRC5) and WT1 are shown in grey for comparison.

Table 1. Compilation of selected phosphopeptides from the expanded dataset that are detected on HLA-A3 and/or HLA-A11, summarizing recurrent presentation patterns.

Modified Sequence	Number of Samples Presented In (Healthy Samples)	Restricting HLA	Source Gene	Presentation in Malignant Tissues
RVAsPTSGVK	15 (3)	A03, A11	IRS2	B-ALL, Melanoma, Ovarian carcinoma, Meningioma, Schwannoma, MCL
SVSsPVKSK*	15 (1)	A03, A11	MGA	EBV-LPD, EBV-BLCL, B-ALL, Melanoma
RTNsPGFQK	12 (0)	A03, A11	RBM26	EBV-LPD, EBV-BLCL, B-ALL, Ovarian carcinoma, Meningioma, BL
HVYtPSTTK	11 (3)	A03, A11	ANKRA2	B-ALL, Melanoma, Meningioma, Schwannoma, AML
RTAsPPPPPK*	11 (0)	A03, A11	SRRM1	EBV-LPD, EBV-BLCL, Melanoma, AML, MCL, BL
KLRsPFLQK	10 (2)	A03, A11	DBNL	B-ALL, Meningioma, AML, BL
KVQGsPLKK	10 (1)	A03, A11	AKAP12	B-ALL, Ovarian carcinoma, Meningioma, Schwannoma
KVSsPTKPK*	10 (1)	A03, A11	GTF3C2	EBV-LPD, EBV-BLCL, B-ALL, Melanoma, Ovarian carcinoma
RAKsPISLK	10 (1)	A03, A11	CARD11	EBV-BLCL, Meningioma, Schwannoma, MCL
RLSsPISKR	10 (1)	A03, A11	BARD1	Melanoma, Ovarian carcinoma, Meningioma, AML, BL

ATAsPPRQK	9 (1)	A11	SRRM2	EBV-LPD, EBV-BLCL, B-ALL, Meningioma
ATQsPISKK*	9 (0)	A03, A11	MYBBP1A	EBV-BLCL, EBV-LPD, B-ALL, Ovarian carcinoma, Meningioma
GSGsPAPPR	9 (1)	A11	GPATCH8	EBV-LPD, EBV-BLCL, B-ALL, Meningioma
SVKsPVTVK	9 (1)	A03, A11	TCF7L1	Meningioma, Melanoma, Schwannoma
RT AsPNRAGK*	3 (0)	A03, A11	HIF1A	EBV-LPD, B-ALL, Melanoma
RTAsPPALPK*	4 (0)	A03, A11	PRDM2	EBV-BLCL, EBV-LPD, Melanoma, BL
HSLsPGPSK*	4 (0)	A11	PIM1	EBV-BLCL, Meningioma
ATPTSPIKK*	8 (0)	A11	PPP1R12A	EBV-BLCL, EBV-LPD, B-ALL, Meningioma, MCL

*Marks phosphopeptides selected for subsequent investigation.

Structural characteristics of phosphopeptide-mhc complexes

Phosphopeptide-MHC complexes are proposed to exhibit immunogenicity due to the phosphate group enhancing both MHC stability and solvent-exposed character. However, this property is not universal; structural analyses of phosphopeptide-HLA-A*02:01 complexes indicate that such effects vary depending on the individual peptide. To investigate whether phosphorylation similarly enhances peptide binding to HLA-A3 molecules, we measured the binding of selected phosphopeptides and their unmodified ("wild-type") counterparts using both in vitro and computational approaches.

Using TAP-deficient T2 cells engineered to express HLA-A*03:01, we observed that all five phosphopeptide-wild-type pairs stabilized HLA-A*03:01 without showing promiscuous binding to HLA-A*02:01. However, phosphorylation did not increase the stabilization of HLA-A*03:01 compared with the corresponding wild-type peptides **(Figures 3a–3c)**. In one instance, the phosphopeptide pMGAP demonstrated reduced stabilization relative to MGAPwt, requiring higher peptide concentrations to achieve similar HLA-A3 stabilization, consistent with previous reports for B*07:02 and B*40:01 phosphopeptides [32, 37].

Docking analyses of each phosphopeptide with its wild-type revealed that in two of five pairs—MYBBP1A and MGAP—the unmodified peptide formed more stable complexes with HLA-A3, as indicated by lower Rosetta energy scores among the top 10 models **(Figure 3d)**. Only the phosphopeptide of SRRM1 formed a notably more stable complex than its wild-type. The remaining pairs, HIF1A and PRDM2, displayed minimal differences in predicted stability. For MGAP, both experimental stabilization and docking data suggest that phosphorylation diminishes peptide-HLA-A3 stability.

Examining the top 10 docking models of pMGAP and MGAPwt revealed highly similar backbone conformations **(Figure 3e)**. The mean number of hydrogen bonds at the peptide-MHC interface was comparable (11.7 for MGAPwt versus 12.1 for pMGAP; two-tailed p=0.39), prompting further analysis of interfacial energetic contributions. Decomposition of the Rosetta energy function into individual terms allowed calculation of ΔΔG between MGAPwt and pMGAP. The largest favorable contribution arose from electrostatic interactions (Δfa_elec, −54.5 kcal/mol), partially offset by an unfavorable solvation term (Δfa_sol, 29.5 kcal/mol) **(Figure 3f).**

Since the only difference between MGAPwt and pMGAP is the presence of a phosphate on P4Ser, we analyzed contacts between P4Ser and HLA residues. In MGAPwt, P4Ser interacts with Asn66, contributing a mean potential of −0.574 kcal/mol. Visualization of P4Ser and Asn66 shows seven van der Waals contacts in MGAPwt/HLA-A3 **(Figure 3h),** (left), whereas these contacts are lost in pMGAP/HLA-A3 due to insufficient proximity **(Figure 3h)**, (right).

Despite this variability, three of the five phosphopeptide-wild-type pairs were observed to be co-presented in mass spectrometry data, demonstrating that HLA-A3 can effectively display both phosphorylated and unmodified peptides.

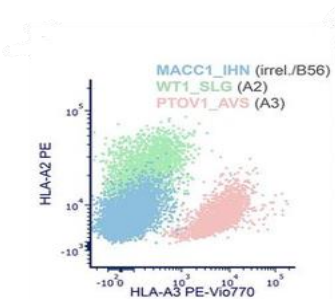

a)

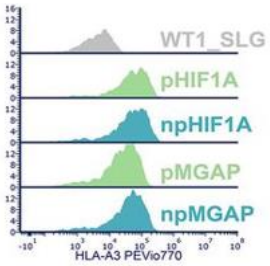

b)

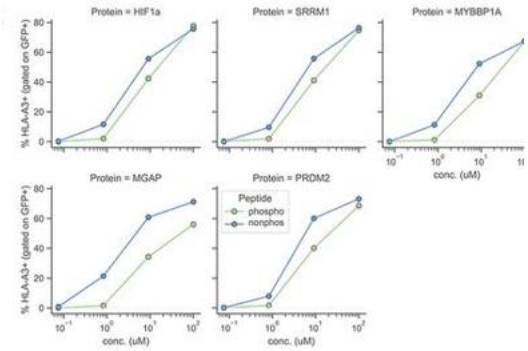

c)

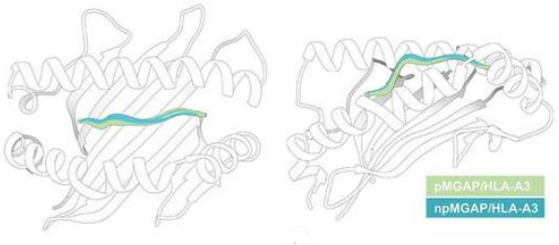

d)

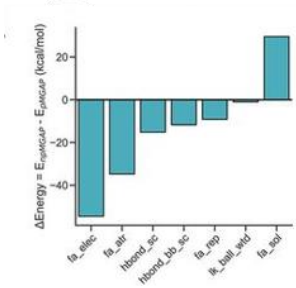

e)

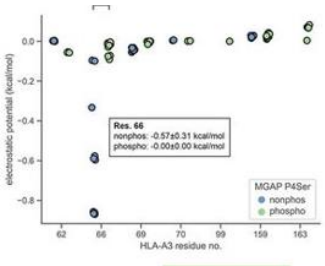

f)

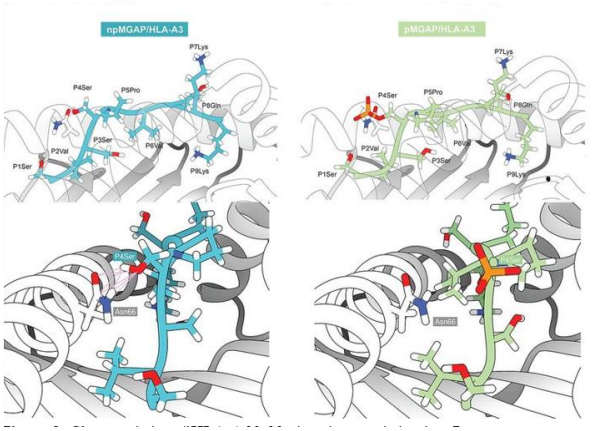

g)

Figure 3. Characteristics of HLA-A*03:01 phosphopeptide binding.

*(a) Assessment of HLA-A*03:01 stabilization using reference peptides: HLA-A3 binder PTOV1, HLA-A2 binder WT1_SLG, and a non-binding control peptide MACC1.

(b) Histograms showing HLA-A3 surface expression on T2-A*03:01 cells pulsed with 100 µg/mL of each indicated peptide.

(c) Dose-dependent stabilization of HLA-A3 in response to titrated phosphopeptide-wild-type pairs.

(d) Rosetta energy scores (in REU) for the top 10 FlexPepDock models of each phosphopeptide-wild-type complex with HLA-A3.

(e) Overlay of peptide backbone conformations for the top 10 models of pMGAP and MGAPwt bound to HLA-A3.

(f) Breakdown of mean ΔΔG contributions from individual Rosetta energy terms between MGAPwt and pMGAP top 10 models shown in panel E.

(g) Electrostatic potentials for all P4Ser interactions with HLA-A3 in pMGAP and MGAPwt.

(h) Visualization of P4Ser contacts with Asn66 in MGAPwt/HLA-A3 (left) and pMGAP/HLA-A3 (right). Pink lines indicate van der Waals overlaps sufficient for contact formation. All statistical analyses used paired t-tests. p-value notation: ns: 5.00e-02 < p ≤ 1.00e+00; *: 1.00e-02 < p ≤ 5.00e-02; **: 1.00e-03 < p ≤ 1.00e-02; ***: 1.00e-04 < p ≤ 1.00e-03; ****: p ≤ 1.00e-04.

HLA-C phosphopeptide presentation and molecular determinants

Given the limited polymorphism of HLA-C relative to HLA-A and -B loci, we next evaluated phosphopeptides presented by common HLA-C alleles as potential tumor

antigens. Phosphopeptides identified on multiple HLA-C*07:01 and HLA-C*07:02 EBV-BLCL lines, tumor samples, and monoallelic cell lines [38] were selected, excluding sequences found in healthy cadaver tissue [39]. Seven phosphopeptides—pRBM14, pRAF1, pMYO9B, pZNF518A, pWNK, pSTMN, and pNCOR—were pulsed onto T2 cells expressing HLA-C*07:01 or C*07:02 to evaluate stabilization. Except for pWNK, all phosphopeptides were detected in immunopeptidomes of both C*07:01+ and C*07:02+ cell lines. However, only C*07:01 was stabilized by these peptides; none stabilized C*07:02 **(Figure 4a)**.

To explore molecular determinants, each 9-mer phosphopeptide was docked onto C*07:01 and C*07:02. Across all complexes, the top 10 models consistently showed greater stability for C*07:01 than C*07:02, indicated by lower Rosetta energy scores **(Figure 4b).** Backbone conformations were largely similar, though C*07:01-bound peptides were slightly more displaced out of the groove **(Figure 4c)**. Buried solvent-accessible surface area (SASA) differed significantly only for pNCOR-bound complexes **(Figure 4d)**. Structural examination of pNCOR revealed that conformational differences were mediated by altered sidechain orientations **(Figure 4e)**.

HLA-C*07:01 and C*07:02 differ only at residues 66 and 99. Analysis suggested that contacts with these residues explain conformational and SASA differences. pNCOR formed 12 hydrogen bonds with C*07:02 and 13 with C*07:01, but only a few were shared. In C*07:01, P2Arg formed two hydrogen bonds with Tyr99 and one with Asp9 in the β-sheet B-pocket. In C*07:02, Ser99 replaced Tyr99, and P2Arg lost these interactions **(Figure 4f)**, leading to compensatory hydrogen bonds with the α1 helix (P1Arg-Glu63 and P4pSer-Arg69). The residue at position 66 made no direct contacts. These alterations rendered the C*07:02-bound peptide more buried and energetically less favorable.

Only 2 of 7 phosphopeptides, pRAF1 and pWNK, were co-presented with their wild-type peptides in MS data. Docking phosphopeptide-wild-type pairs to C*07:01 showed no significant differences in energy or backbone conformation (data not shown). That 5 of 7 tumor-expressed phosphopeptides bound C*07:01 without co-presentation of their wild-type counterparts indicates abundant phosphopeptide presentation by C*07:01, consistent with prior observations [32].

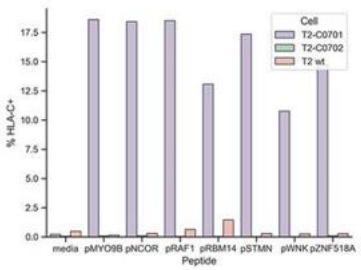

a)

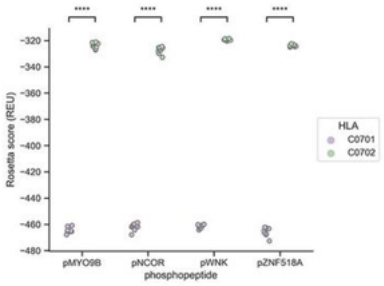

b)

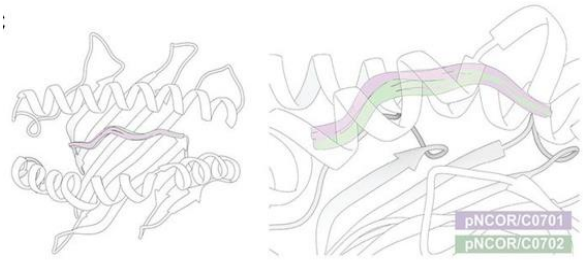

c)

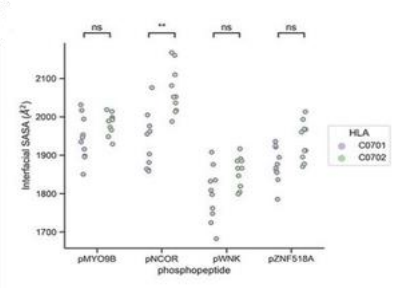

d)

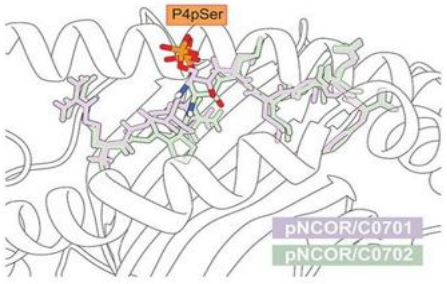

e)

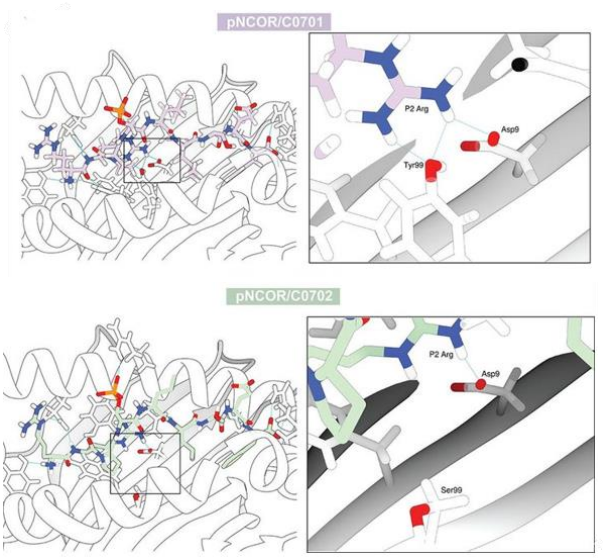

f)

Figure 4. Binding characteristics of phosphopeptides to HLA-C7.

(a) Measurement of HLA-C stabilization on T2 cells expressing C*07:01, C*07:02, or wild-type after incubation with 100 µg/mL of the listed phosphopeptides.

(b) Energy scores (Rosetta REU) for the top 10 docking models of each phosphopeptide bound to HLA-C*07:01 and C*07:02 using FlexPepDock.

(c) Comparison of peptide backbone conformations for the top 10 models of pNCOR in complex with C*07:01 versus C*07:02.

(d) Buried solvent-accessible surface area (SASA) at the peptide-HLA interface for each phosphopeptide in C*07:01 and C*07:02.

(e) Representative sidechain arrangements of pNCOR bound to C*07:01 and C*07:02.

(f) Hydrogen bonding between P2Arg and Tyr99 in pNCOR/C*07:01 (top) and lack of hydrogen bonds with Ser99 in pNCOR/C*07:02 (bottom). All statistical comparisons were performed using paired t-tests. p-value notation: ns: 5.00e-02 < p ≤ 1.00e+00; *: 1.00e-02 < p ≤ 5.00e-02; **: 1.00e-03 < p ≤ 1.00e-02; ***: 1.00e-04 < p ≤ 1.00e-03; ****: p ≤ 1.00e-04.

Evaluation of phosphopeptide immunogenicity

In healthy donors, T cell responses to phosphopeptides presented by HLA-A*02:01 primarily derive from memory T cells rather than naïve populations, contrasting with typical self-antigen responses [10, 34]. To examine phosphopeptide-specific cytotoxic T cells (PP-CTL), we generated dextramers using an optimized assembly approach [28]. Dextramers included six selected phosphopeptides and an irrelevant HLA-A2-binding control peptide, WT1_SLG. Fluorophore barcoding [40] allowed discrimination between phosphopeptide-specific and WT1-specific T cells **(Figure 5a)**.

PBMC from A*02:01+ donors were exposed to T2-A*02:01 cells pulsed with the six phosphopeptides. After 10 days, ~4% of CD8+ T cells bound phosphopeptide dextramers without cross-reactivity to WT1_SLG. PBMC simultaneously stimulated with WT1_SLG-pulsed T2 cells did not generate T cells recognizing either WT1_SLG or phosphopeptides **(Figure 5b)**, indicating that phosphopeptides induce a stronger T cell response despite similar HLA-A2 stabilization.

Sequential magnetic enrichment of PBMC from two additional donors yielded highly pure PP-CTL populations (>95% dextramer-positive) **(Figure 5c).** Effector function was assessed by IFNγ ELISpot. Across four donors, responses were observed against pIRS2 and pCDC25B, with pCDC25B-specific responses being strictly phosphorylation-dependent **(Figures 5d and 5e).**

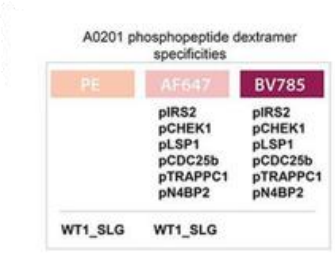

a)

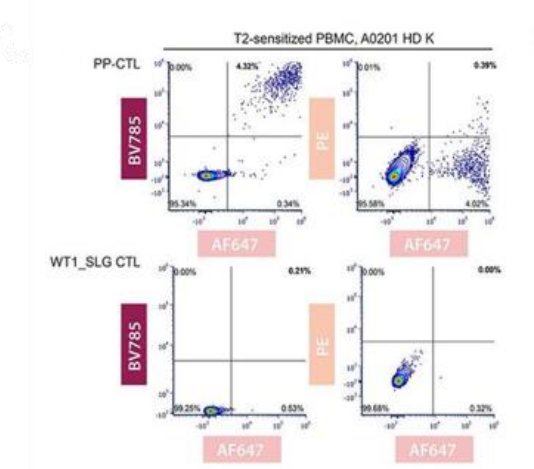

b)

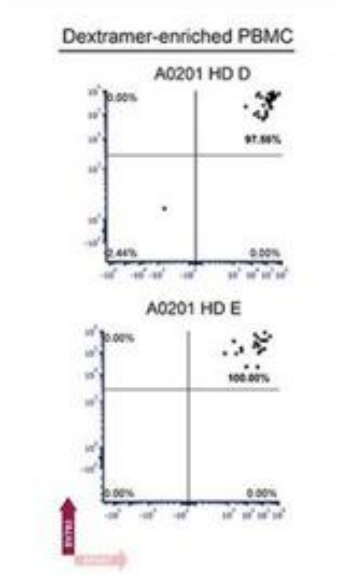
Dextramer-enriched PBMC
A0201 HD D
97.56%
2.44%
0.00%
A0201 HD E
100.00%
0.00%
0.00%

c)

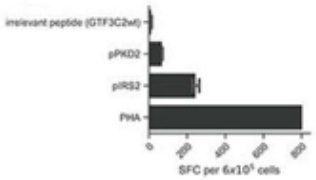
irrelevant peptide (GTF3C2wt)
pPKD2
pIRS2
PHA
SFC per 6x10^5 cells

d)

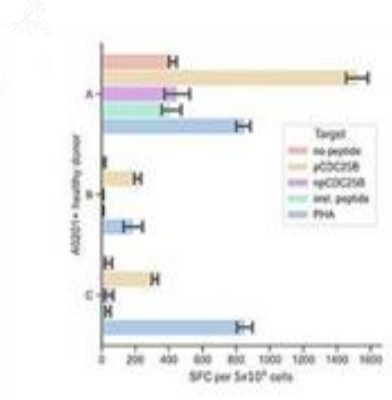
A0201+ healthy donor
Target
no peptide
pGTF3C2
npGTF3C2
irrel. peptide
PHA
SFC per 5x10^5 cells

e)

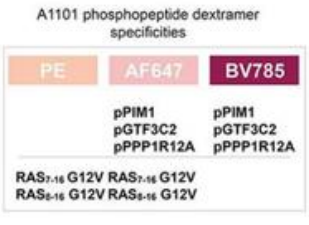
A1101 phosphopeptide dextramer specificities
PE
AF647
BV785
pPIM1
pGTF3C2
pPPP1R12A
RAS7-16 G12V RAS7-16 G12V
RAS8-16 G12V RAS8-16 G12V

f)

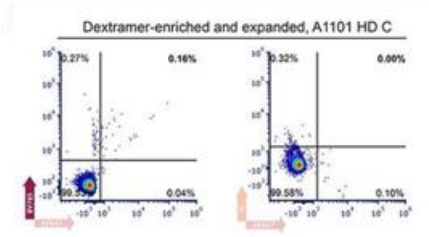
Dextramer-enriched and expanded, A1101 HD C
0.27%
0.16%
0.04%
0.32%
0.00%
99.58%
0.10%

g)

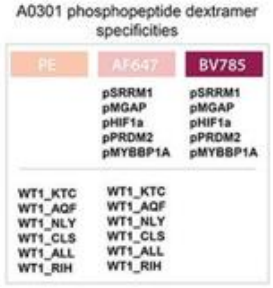
A0301 phosphopeptide dextramer specificities
PE
AF647
BV785
pSRRM1
pMGAP
pHIF1a
pPRDM2
pMYBBP1A
WT1_KTC
WT1_AQF
WT1_NLY
WT1_CLS
WT1_ALL
WT1_RIH

h)

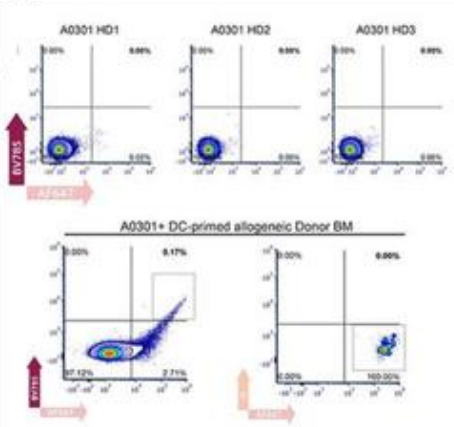
A0301 HD1
A0301 HD2
A0301 HD3
BV785
AF647
A0301+ DC-primed allogeneic Donor BM
97.12%
2.71%
0.00%
100.00%

i)

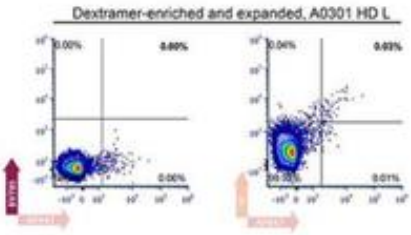
Dextramer-enriched and expanded, A0301 HD L
0.00%
0.00%
0.00%
0.04%
0.03%
99.96%
0.01%

j)

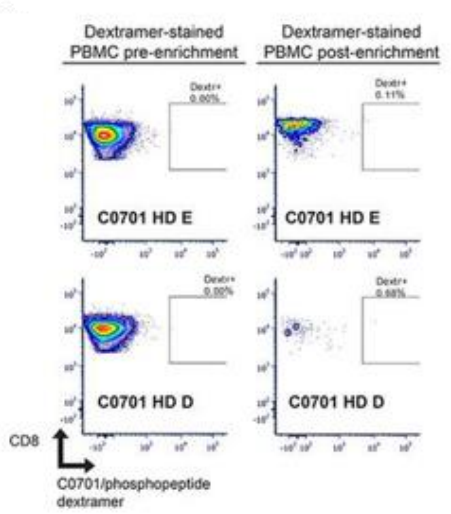

k)

Figure 5. Fluorophore barcoded dextramer analysis of PP-CTL responses.

(a) HLA-A*02:01 dextramer panel where phosphopeptide-bound HLA-A2 dextramers are tagged with AF647/BV785, and A2/WT1_SLG dextramers use PE/AF647.*

*(b) T cells from A*02:01+ donor were sensitized with either phosphopeptides (top) or WT1_SLG (bottom). PP-CTL (top) is detected using A2/phosphopeptide dextramer (AF647/BV785), showing no cross-reactivity with A2/WT1_SLG dextramer in the PE/AF647 channel.

(c) Sequential enrichment of PP-CTL from A*02:01+ donor buffy coats using dextramer on two magnetic columns, followed by flow cytometry analysis.*

*(d) ELISpot assays measuring IFN-γ production in T cells from A*02:01+ donors exposed to pPKD2 and pIRS2 phosphopeptides. PHA serves as a positive control, with GTF3C2wt peptide used as the negative control.

(e) ELISpot analysis of T cells from three A*02:01+ donors (labeled A, B, C) sensitized to pCDC25B, followed by re-challenge with autologous CD14+ cells pulsed with the peptides indicated in the "Target" section. PHA serves as a positive control.*

*(f) Panel for A*11:01 dextramer analysis, using phosphopeptides in BV785/AF647 and RAS G12V peptides in PE/AF647.

(g) PBMC from an A*11:01+ donor were enriched and expanded using dextramer for PP-CTL detection, showing binding to A*11:01/phosphopeptide dextramer (AF647/BV785), with no binding to irrelevant RAS G12V dextramer (PE/AF647).

(h) Panel for HLA-A*03:01 dextramer, using phosphopeptides in AF647/BV785 and WT1 epitopes for irrelevant control in PE/AF647.*

*(i) For three A*03:01+ donors, no PP-CTL response was seen after priming with phosphopeptide-pulsed autologous DCs, but when A*03:01-negative donor BMMC cells were exposed to allogeneic A*03:01+ DCs, PP-CTL were generated, binding to A3/phosphopeptide dextramer but not A3/WT1.

(j) Following dextramer enrichment, a small population of WT1-specific T cells was observed in a co-enrichment scheme involving WT1/phosphopeptide fluorochrome (AF647), while no PP-CTL were expanded.

(k) Analysis of C*07:01 phosphopeptides showed no observable PP-CTL in healthy C*07:01 donor PBMC before or after dextramer enrichment.

(l) Iterative dextramer enrichment and expansion using C*07:01-negative donors generated a significant population of T cells recognizing C*07:01/phosphopeptide dextramer using dual fluorochromes (PE/PECy5). All data were gated on live, CD8+ CD19-CD14-CD123-CD40- single cells.

Immunogenicity of PP-CTL

Given the responses to certain A*11:01 phosphopeptides, we constructed an A*11:01 dextramer panel containing both phosphopeptide-specific and irrelevant RAS G12V peptide-specific controls **(Figure 5f)**. After enriching PBMC from A*11:01+ healthy donors, a small population of PP-CTL was identified that did not cross-react with the RAS G12V dextramer* **(Figure 5g).** *However, in two additional A*11:01+ donors, we were unable to detect PP-CTL after sequential magnetic enrichment (data not shown). This suggests that A*11:01 phosphopeptides are less frequently recognized compared to those presented by A*02:01.

To assess A*03:01 phosphopeptide immunogenicity, we used dextramers for shared phosphopeptides identified from our analysis* **(Table 1),** *along with A3-binding WT1 epitopes as controls* **(Figure 5h)**. *After enrichment from A*03:01+ donors, no PP-CTL responses were detected, even after sensitization with autologous DCs or repeated exposure to phosphopeptide-pulsed T2-A0301 cells (data not shown). However, PP-CTL responses were observed after priming A*03:01-negative donor T cells with A*03:01+ DCs loaded with phosphopeptides, showing specificity for A3/phosphopeptide dextramer and no cross-reactivity with A3/WT1 dextramer **(Figure 5i).**

A*03:01 phosphopeptides elicited weaker immune responses compared to A*02:01 and A*11:01 phosphopeptides, requiring allogeneic T cell stimulation from A*03:01-negative donors to generate a detectable response.

For C*07:01 phosphopeptides, we constructed a dextramer pool containing pRBM14, pRAF1, pMYO9B, and others. No PP-CTL responses were detected in two C*07:01 healthy donor buffy coats, either before or after dextramer enrichment **(Figure 5k)**. However, using iterative enrichment and expansion in C*07:01-negative donors, we generated a significant population of T cells recognizing the C*07:01/phosphopeptide dextramer **(Figure 5l).** These findings suggest that, despite the high abundance of C*07:01 phosphopeptides in the immunopeptidome [32], they do not induce robust T cell responses in the autologous setting compared to other HLA alleles like A*03:01.

Phosphopeptides constitute a growing class of HLA ligands with potential as shared tumor antigens, arising from cancer-associated post-translational modifications rather than genetic mutations. While T cell recognition of phosphopeptides has been extensively characterized for HLA-A*02:01 and HLA-B*07:02 [10, 34, 41], we aimed to broaden this landscape by systematically reanalyzing large immunopeptidomic datasets to uncover phosphopeptides presented by the HLA-A3 supertype and HLA-C*07:01. To assess their tumor specificity, we cross-referenced these peptides with healthy tissue databases [40]. We observed phosphopeptides that follow HLA-A3 supertype binding preferences yet are presented exclusively by malignant cells, supporting their utility as tumor antigens across multiple HLA alleles. Supertype cross-reactivity has been described previously, for instance, pIRS2 binding A*02:01 and A*68:02, with length variants also engaging A*03:01 and A*11:01 [42]. Notably, although abnormal phosphorylation is a hallmark of cancer, the phosphopeptides we identified largely originate from fundamental cellular pathways like nucleic acid binding and repair, rather than oncogenic kinase signaling. Differences in phosphopeptide presentation have been attributed more to inhibition of key phosphatases than to kinase overactivation [42].

Using TAP-deficient cell lines, we validated that MS-identified phosphopeptides could stabilize their respective HLA alleles. All phosphopeptides chosen for A*03:01 and C*07:01 bound their cognate alleles; however, no phosphopeptide conferred a binding advantage relative to its unmodified counterpart for A*03:01. Previous studies found enhanced half-lives or IC50 for only 1/5 HLA-A*01:01 peptides, 0/5 HLA-B*07:02 peptides, and 0/7 HLA-B*40:02 peptides [32,37], contrasting with HLA-A2, where phosphorylation increased peptide affinity 1.1–158.6-fold in 10/11 cases [9]. Differences in binding behavior between alleles may partly reflect technical limitations: DDA-mode MS favors charged peptides that fragment efficiently, while HLA-A2 prefers hydrophobic anchors, potentially enriching phosphopeptides with suboptimal anchors that require phosphorylation for stable HLA binding. This may explain why some phosphopeptide-wild-type pairs are co-presented by HLA-A3, which favors charged anchors. Notably, phosphopeptides more often exhibited improved binding to HLA-C*07:02 and C*06:02 than to HLA-A and -B alleles [32]. In our dataset, most C*07:01 phosphopeptides were not co-presented with wild-type peptides, and docking analyses showed no energetic difference for the two pairs that were co-presented, suggesting the phosphopeptide is generally the more abundant species. These observations underscore the importance of considering HLA allele-specific anchor preferences when selecting phosphopeptides for enhanced binding.

Our docking studies revealed that sidechain interactions with the HLA B-pocket and α1 helix are key determinants of phosphopeptide binding to HLA-A3 and C7. In HLA-A*02:01, phosphate-mediated contacts with Arg65 of the α1 helix were previously shown to enhance binding [9], and for HLA-B*07:02, the phosphate was positioned within hydrogen-bond distance to Arg62 [43]. For HLA-A*03:01, wild-type P4Ser formed more favorable contacts with Asn66 of the α1 helix than phosphoserine, explaining the reduced stabilization observed for pMGAP. In the HLA-C*07 comparison, Tyr99 of C*07:01 established hydrogen bonds with P2Arg, absent in C*07:02 due to the Ser99 substitution [44]. This demonstrates that B-pocket and α1 helix interactions are sensitive to subtle changes, including phosphate addition or single residue substitutions. However, our docking predictions lack explicit solvent effects, which would be captured in crystallography or explicit-solvent molecular dynamics simulations.

A major advantage of phosphopeptides for immunotherapy is that phosphorylation generates a unique recognition surface distinct from the wild-type sequence. Prior work has shown that T cells, TCRs, and

TCR-mimicking antibodies can specifically recognize phosphopeptides presented by HLA without crossreacting with wild-type peptides [10, 17, 44, 45]. Conversely, class II-restricted pWED-specific T cells did not distinguish phosphorylated from unmodified peptides [46]. This highlights that TCR-like agents can be designed for phosphorylation-specific recognition, but achieving such specificity in native T cells requires rigorous methodological approaches.

Our research highlights that phosphopeptides can act as broadly shared tumor antigens, but differences between HLA alleles must be carefully accounted for in immunotherapy development. For example, both A*03:01 and B*07:02 exhibit similar patterns of co-presenting phosphopeptide-wild-type pairs, whereas A*02:01 generally favors binding to phosphopeptides. Despite this, phosphopeptides restricted by A*02:01 and B*07:02 are more consistently recognized by autologous T cells compared to those restricted by A*03:01. Therefore, targeting A*03:01-restricted phosphopeptides may require strategies such as allogeneic T cell stimulation, engineered TCRs, or TCR-mimicking antibodies to engage immune effector functions.

- What is already known on this topic – Phosphorylated peptides bound by common HLA alleles like A*02:01 and B*07:02 are displayed across multiple tumor types, show structural advantages due to phosphorylation, and are recognized by T cells from healthy individuals. Whether these properties extend to phosphopeptides presented by other widely expressed alleles remains unclear.
- What this study adds – We evaluated phosphopeptide presentation, binding affinity, structural characteristics, and T cell immunogenicity for the prevalent alleles A*03:01, A*11:01, C*07:01, and C*07:02. These alleles were selected because the phosphopeptides were detected on malignant but not normal cells. We identified tumor antigens originating from genes essential for leukemia and lymphoma survival that can bind A3, A11, and C7 molecules. While circulating T cell responses to phosphopeptides were detected for A*02:01 and A*11:01 in healthy donors, responses to A*03:01 or C*07:01 phosphopeptides were only apparent when using allogeneic donor T cells, suggesting limited natural immunogenicity but potential for targeted therapies.
- How this study might affect research, practice, or policy – The phosphopeptide targets identified here can guide immunotherapy approaches for patients with HLA alleles beyond A*02:01, provided that the allele-specific differences we describe are incorporated into therapeutic design.

Acknowledgments: We thank the Dr. Henrik Molina of the Proteomics Resource Center at Rockefeller University for the performance of all LC/MS-MS experiments. Molecular graphics and analyses performed with UCSF Chimera, developed by the Resource for Biocomputing, Visualization, and Informatics at the UCSF, with support from NIH P41-GM103311. We acknowledge the use of the MSK Flow Cytometry Core Facility, funded in part through the NIH/NCI Cancer Center Support Grant P30 CA008748. We thank Dr. Joshua Elias (Chan Zuckerberg Biohub, Stanford, CA, USA) for providing HLA typing of samples from PXD004746 and PXD005704.

Conflict of Interest: DAS is on a board of, or has equity in, or income from: Lantheus, Sellas, Iovance, Pfizer, Actinium Pharmaceuticals, Inc., OncoPep, Repertoire, Sapience, and Eureka Therapeutics. TD is a consultant for Eureka Therapeutics. MGK is a consultant to Ardigen. RJO declares consultancy, research support, and royalties from Atara Biotherapeutics. All other authors declare no competing financial interests.

Financial Support: ZM and RJO acknowledge support from the Steven A. Greenberg Lymphoma Research Award (GC-242236) and Alex's Lemonade Stand Foundation Innovation Award (GR-000002624). RJO was supported by NIH NCI P01 CA023766, NCI Cancer Center support grant P30 CA008748, Richard "Rick" J. Eisemann Pediatric Research Fund, The Tow Foundation, The Aubrey Fund, and Edith Robertson Foundation. DAS was supported by NIH NCI P01 CA23766 and R35 CA241894. TD was supported by NCI 1R50CA265328. MGK is participant in the BIH Charité Clinician Scientist Program funded by the Charité – Universitätsmedizin Berlin, and the Berlin Institute of Health at Charité (BIH).

Ethics Statement: Written informed consent was received from participants prior to inclusion in the study. Use of human blood samples was approved by MSKCC IRB protocol #06–107.

References

1. Hont AB, Cruz CR, Ulrey R, et al. Immunotherapy of Relapsed and Refractory Solid Tumors With Ex Vivo Expanded Multi-Tumor Associated Antigen Specific Cytotoxic T Lymphocytes: A Phase I Study. J Clin Oncol 2019;37:2349. doi: 10.1200/JCO.19.00177
2. Lulla PD, Naik S, Vasileiou S, et al. Clinical effects of administering leukemia-specific donor T cells to patients with AML/MDS after allogeneic transplant. Blood 2021;137:2585–97. doi: 10.1182/blood.2020009471
3. Molvi Z, O'Reilly RJ. Allogeneic Tumor Antigen-Specific T Cells for Broadly Applicable Adoptive Cell Therapy of Cancer BT - Cancer Immunotherapies: Solid Tumors and Hematologic Malignancies. In: Hays P, ed. . Cham: : Springer International Publishing; 2022. 131–59. doi: 10.1007/978-3-030-96376-7_4
4. Bassani-Sternberg M, Bräunlein E, Klar R, et al. Direct identification of clinically relevant neoepitopes presented on native human melanoma tissue by mass spectrometry. Nat Commun 2016;7:13404. doi: 10.1038/ncomms13404
5. Zarling AL, Ficarro SB, White FM, et al. Phosphorylated Peptides Are Naturally Processed and Presented by Major Histocompatibility Complex Class I Molecules In Vivo. J Exp Med 2000;120800:1755–62. doi: 10.1084/jem.192.12.1755
6. Malaker SA, Penny SA, Steadman LG, et al. Identification of Glycopeptides as Posttranslationally Modified Neoantigens in Leukemia. Cancer Immunol Res 2017;5:376–84. doi: 10.1158/2326-6066.CIR-16-0280
7. Zarling AL, Polefrone JM, Evans AM, et al. Identification of class I MHC-associated phosphopeptides as targets for cancer immunotherapy. Proc Natl Acad Sci 2006;103:14889–94. doi: 10.1073/pnas.0604045103
8. Depontieu FR, Qian J, Zarling AL, et al. Identification of tumor-associated, MHC class II-restricted phosphopeptides as targets for immunotherapy. Proc Natl Acad Sci U S A 2009;106:12073–8. doi: 10.1073/pnas.0903852106
9. Mohammed F, Cobbold M, Zarling AL, et al. Phosphorylation-dependent interaction between antigenic peptides and MHC class I: A molecular basis for the presentation of transformed self. Nat Immunol 2008;9:1236–43. doi: 10.1038/ni.1660
10. Cobbold M, De La Peña H, Norris A, et al. MHC class I-associated phosphopeptides are the targets of memory-like immunity in leukemia. Sci Transl Med 2013;5:1–11. doi: 10.1126/scitranslmed.3006061
11. Penny SA, Abelin JG, Malaker SA, et al. Tumor Infiltrating Lymphocytes Target HLA-I Phosphopeptides Derived From Cancer Signaling in Colorectal Cancer . Front. Immunol. . 2021;12.
12. Cafri G, Yossef R, Pasetto A, et al. Memory T cells targeting oncogenic mutations detected in peripheral blood of epithelial cancer patients. Nat Commun 2019;10:449. doi: 10.1038/s41467-019-08304-z
13. Liu S, Matsuzaki J, Wei L, et al. Efficient identification of neoantigen-specific T-cell responses in advanced human ovarian cancer. J Immunother Cancer 2019 71 2019;7:1–17. doi: 10.1186/S40425-019-0629-6
14. Kowarz E, Löscher D, Marschalek R. Optimized Sleeping Beauty transposons rapidly generate stable transgenic cell lines. Biotechnol J 2015;10:647–53. doi: 10.1002/BIOT.201400821
15. Mátés L, Chuah MKL, Belay E, et al. Molecular evolution of a novel hyperactive Sleeping Beauty transposase enables robust stable gene transfer in vertebrates. Nat Genet 2009;41:753–61. doi: 10.1038/NG.343
16. Klatt MG, MacK KN, Bai Y, et al. Solving an MHC allele–specific bias in the reported immunopeptidome. JCI Insight 2020;5. doi: 10.1172/JCI.INSIGHT.141264
17. Dao T, Mun SS, Molvi Z, et al. A TCR mimic monoclonal antibody reactive with the "public" phospho-neoantigen pIRS2/HLA-A*02:01 complex. JCI Insight 2022;7. doi: 10.1172/jci.insight.151624
18. Pettersen EF, Goddard TD, Huang CC, et al. UCSF Chimera--a visualization system for exploratory research and analysis. J Comput Chem 2004;25:1605–12. doi: 10.1002/jcc.20084
19. Shapovalov MV, Dunbrack RL. A Smoothed Backbone-Dependent Rotamer Library for Proteins Derived from Adaptive Kernel Density Estimates and Regressions. Structure 2011;19:844–58. doi: 10.1016/j.str.2011.03.019
20. Gfeller D, Michielin O, Zoete V. SwissSidechain: a molecular and structural database of non-natural

sidechains. Nucleic Acids Res 2013;41:D327–32. doi: 10.1093/nar/gks991
21. Raveh B, London N, Schueler-Furman O. Sub-angstrom modeling of complexes between flexible peptides and globular proteins. Proteins 2010;78:2029–40. doi: 10.1002/prot.22716
22. Leaver-Fay A, Tyka M, Lewis SM, et al. Rosetta3: An Object-Oriented Software Suite for the Simulation and Design of Macromolecules. In: Johnson ML, Brand LBT-M in E, eds. Computer Methods, Part C. Academic Press; 2011. 545–74. doi: 10.1016/B978-0-12-381270-4.00019-6
23. Wölfl M, Greenberg PD. Antigen-specific activation and cytokine-facilitated expansion of naive, human CD8+ T cells. Nat Protoc 2014;9:950–66. doi: 10.1038/nprot.2014.064
24. May RJ, Dao T, Pinilla-Ibarz J, et al. Peptide epitopes from the Wilms' tumor 1 oncoprotein stimulate CD4 + and CD8+ T cells that recognize and kill human malignant mesothelioma tumor cells. Clin Cancer Res 2007;13:4547–55. doi: 10.1158/1078-0432.CCR-07-0708
25. Pinilla-Ibarz J, May RJ, Korontsvit T, et al. Improved human T-cell responses against synthetic HLA-0201 analog peptides derived from the WT1 oncoprotein. Leukemia 2006;20:2025–33. doi: 10.1038/sj.leu.2404380
26. G D K, A L T, et al. More tricks with tetramers: a practical guide to staining T cells with peptide-MHC multimers. Immunology 2015;146:11–22. doi: 10.1111/IMM.12499
27. Molvi Z. Peptide-MHC Dextramer Assembly. protocols.io 2022.
28. 2Bethune MT, Comin-Anduix B, Fu Y-HH, et al. Preparation of peptide–MHC and T-cell receptor dextramers by biotinylated dextran doping. Biotechniques 2017;62:123–30. doi: 10.2144/000114525
29. Tsherniak A, Vazquez F, Montgomery PG, et al. Defining a Cancer Dependency Map. Cell 2017;170:564–576.e16. doi: 10.1016/j.cell.2017.06.010
30. Narayan R, Olsson N, Wagar LE, et al. Acute myeloid leukemia immunopeptidome reveals HLA presentation of mutated nucleophosmin. PLoS One 2019;14:e0219547.
31. Khodadoust MS, Olsson N, Wagar LE, et al. Antigen presentation profiling reveals recognition of lymphoma immunoglobulin neoantigens. Nature 2017;543:723–7. doi: 10.1038/nature21433
32. Solleder M, Guillaume P, Racle J, et al. Mass spectrometry based immunopeptidomics leads to robust predictions of phosphorylated HLA class I ligands. Mol & Cell Proteomics 2019;:mcp.TIR119.001641. doi: 10.1074/mcp.TIR119.001641
33. Bern M, Kil YJ, Becker C. Byonic: Advanced Peptide and Protein Identification Software. Curr Protoc Bioinforma 2012;40:13.20.1–13.20.14. doi: 10.1002/0471250953.bi1320s40
34. 34.Lulu AM, Cummings KL, Jeffery ED, et al. Characteristics of immune memory and effector activity to cancer-expressed MHC class i phosphopeptides differ in healthy donors and ovarian cancer patients. Cancer Immunol Res 2021;9:1327–41. doi: 10.1158/2326-6066.CIR-21-0111/665806/AM/CHARACTERISTICS-OF-IMMUNE-MEMORY-AND-EFFECTOR
35. Sarkizova S, Klaeger S, Le PM, et al. A large peptidome dataset improves HLA class I epitope prediction across most of the human population. Nat Biotechnol 2020;38:199–209. doi: 10.1038/s41587-019-0322-9
36. Kuleshov M V, Xie Z, London ABK, et al. KEA3: improved kinase enrichment analysis via data integration. Nucleic Acids Res 2021;49:W304–16. doi: 10.1093/nar/gkab359
37. Alpízar A, Marino F, Ramos-Fernández A, et al. A Molecular Basis for the Presentation of Phosphorylated Peptides by HLA-B Antigens. Mol Cell Proteomics 2017;16:181–93. doi: 10.1074/mcp.M116.063800
38. Di Marco M, Schuster H, Backert L, et al. Unveiling the Peptide Motifs of HLA-C and HLA-G from Naturally Presented Peptides and Generation of Binding Prediction Matrices. J Immunol 2017;199:2639–51. doi: 10.4049/jimmunol.1700938
39. Marcu A, Bichmann L, Kuchenbecker L, et al. HLA Ligand Atlas: a benign reference of HLA-presented peptides to improve T-cell-based cancer immunotherapy. J Immunother Cancer 2021;9:e002071. doi: 10.1136/JITC-2020-002071
40. Hadrup SR, Bakker AH, Shu CJ, et al. Parallel detection of antigen-specific T-cell responses by multidimensional encoding of MHC multimers. Nat

Methods 2009 67 2009;6:520–6. doi: 10.1038/nmeth.1345

41. Engelhard VH, Obeng RC, Cummings KL, et al. MHC-restricted phosphopeptide antigens: preclinical validation and first-in-humans clinical trial in participants with high-risk melanoma. J Immunother Cancer 2020;8:e000262. doi: 10.1136/jitc-2019-000262
42. Mahoney KE, Shabanowitz J, Hunt DF. MHC Phosphopeptides: Promising Targets for Immunotherapy of Cancer and Other Chronic Diseases. Mol Cell Proteomics 2021;20:100112. doi: 10.1016/J.MCPRO.2021.100112
43. Patskovsky Y, Natarajan A, Nyovanie S, et al. Molecular mechanism of phosphopeptide neoantigen immunogenicity. Published Online First: 1 December 2022. doi: 10.21203/RS.3.RS-2327641/V1
44. Rasmussen M, Harndahl M, Stryhn A, et al. Uncovering the Peptide-Binding Specificities of HLA-C: A General Strategy To Determine the Specificity of Any MHC Class I Molecule. J Immunol 2014;193:4790–802. doi: 10.4049/jimmunol.1401689
45. Mohammed F, Stones DH, Zarling AL, et al. The antigenic identity of human class I MHC phosphopeptides is critically dependent upon phosphorylation status. Oncotarget 2017;8:54160–72. doi: 10.18632/oncotarget.16952
46. Longino N V, Yang J, Iyer JG, et al. Human CD4+ T Cells Specific for Merkel Cell Polyomavirus Localize to Merkel Cell Carcinomas and Target a Required Oncogenic Domain. Cancer Immunol Res 2019;7:1727–39. doi: 10.1158/2326-6066.CIR-19-0103